HHS Public Access

Author manuscript

J Magn Reson Imaging. Author manuscript; available in PMC 2021 November 01.

Published in final edited form as:

J Magn Reson Imaging. 2020 November ; 52(5): 1510–1524. doi:10.1002/jmri.27240.

Clinical value of non-contrast-enhanced radial quiescent-interval slice-selective (QISS) magnetic resonance angiography for the diagnosis of acute pulmonary embolism compared to contrast-enhanced computed tomography and Cartesian balanced steady-state free precession

Mona Salehi Ravesh, PhD[1,2,*], **Karolin Tesch**[2,*], **Annett Lebenatus, MD**[2], **Ioannis Koktzoglou, PhD**[3,4], **Robert R. Edelman, MD**[3,5], **Matthias Eden, MD**[6], **Patrick Langguth, MD**[2], **Joachim Graessner, MSc**[7], **Olav Jansen, MD**[2], **Marcus Both, MD**[2]

[1]Section Biomedical Imaging, Molecular Imaging North Competence Center (MOIN CC), Department of Radiology and Neuroradiology, University Medical Center Schleswig-Holstein (UKSH), Kiel University, Kiel, Germany

[2]Department of Radiology and Neuroradiology, University Medical Center Schleswig-Holstein (UKSH), Kiel University, Kiel, Germany

[3]Department of Radiology, NorthShore University HealthSystem, Evanston, Illinois, USA

[4]Pritzker School of Medicine, University of Chicago, Chicago, Illinois, USA

[5]Northwestern University Feinberg School of Medicine, Chicago, Illinois, USA

[6]Department for Internal Medicine III, Molecular Cardiology and Angiology, University Hospital Schleswig-Holstein, Campus Kiel, Germany

[7]Siemens Healthcare GmbH, Hamburg, Germany

Abstract

Background: Free-breathing non-contrast-enhanced (non-CE) magnetic resonance angiography (MRA) techniques are of considerable interest for the diagnosis of acute pulmonary embolism (APE) owing to the possibility for repeated examinations, avoidance of side effects from iodine-based contrast agents, and absence of ionizing radiation exposure as compared to CE-computed tomographic angiography (CTA).

Purpose: To analyze the clinical performance of free-breathing and electrocardiogram (ECG) gated radial quiescent-interval slice-selective (QISS)-MRA compared to CE-CTA and to Cartesian balanced steady-state free precession (bSSFP)-MRA.

Study Type: Prospective.

Corresponding Author Info: Mona Salehi Ravesh, PhD, Department of Radiology and Neuroradiology, University Medical Center Schleswig-Holstein (UKSH), Kiel University, Arnold Heller street 3, Building 41, 24105 Kiel, Germany, phone: +49 431 500 16537, Mona.Salehiravesh@uksh.de.

*Dr. Mona Salehi Ravesh and Karolin Tesch contributed equally to this work.

Conflict of interest The authors declare that they have no conflict of interest.

Subjects: 30 patients with confirmed APE and 30 healthy volunteers (HVs).

Field Strength/Sequence: Radial QISS- and bSSFP-MRA at 1.5 Tesla.

Assessment: Signal-to-noise ratio (SNR) and contrast-to-noise ratio (CNR) were computed to compare of pulmonary imaging quality between MRA methods. The pulmonary arterial tree was divided into 25 branches and an ordinal scoring system was used to assess the image quality of each pulmonary branch. The clinical performance of the two MRA techniques in accurately assessing APE was evaluated with respect to CE-CTA as clinical reference standard.

Statistical Tests: Wilcoxon signed-rank- and Spearman's correlation-tests were performed. Sensitivity and specificity of the MRA techniques were determined using CE-CTA as clinical reference standard.

Results: Thrombus-mimicking artifacts appeared more frequently in lobar and peripheral arteries of patients with Cartesian bSSFP than with radial QISS-MRA (pulmonary trunk: 12.2% vs. 14.0%, p=0.64; lobar arteries: 35.6% vs. 22.0%, p=0.005, peripheral arteries: 74.4% vs. 49.0%, p<0.001). The relative increases in SNR and of CNR provided by radial QISS-MRA with respect to Cartesian bSSFP-MRA were 30-35% (p-values of SNR/CNR, HVs: 0.09/0.09, patients: 0.03/0.02). The image quality of pulmonary arterial branches was considered good to excellent in 77.2% of patients with radial QISS-MRA and in 43.2% with Cartesian bSSFP-MRA (p<0.0001). Clinical performance of radial QISS-MRA was higher than Cartesian bSSFP-MRA for grading embolism with a total sensitivity of 86.0% versus 80.6% and a specificity of 93.3% versus 84.0%, respectively.

Data Conclusion: Radial QISS-MRA is a reliable and safe non-CE angiographic technique with promising clinical potential compared to Cartesian bSSFP-MRA and is an alternative technique to CE-CTA for the diagnosis of APE.

Keywords

Acute pulmonary embolism; Non-contrast-enhanced radial quiescent-interval; Slice-selective (QISS); Free-breathing; Cartesian balanced steady-state free precession; Contrast-enhanced computed tomography

Introduction

Acute pulmonary embolism (APE) is characterized by embolic occlusion of one or more pulmonary arteries, which results in potential circulatory failure, subsequent pulmonary hypertension, right ventricular failure, pulmonary infarction, and also irreversible multi-organ impairment due to restricted blood flow and oxygen supply [1, 2]. Therefore, it is a potentially life-threatening condition that requires urgent diagnosis and rapid, appropriate treatment. APE is most commonly induced by deep venous thrombosis in the lower extremities. Typical risk factors are surgical procedures, immobilization, cancer, hormonal contraceptives, pregnancy, smoking, and hereditary blood clotting disorders [2].

While perfusion-ventilation scintigraphy remains the imaging modality of choice for chronic thromboembolic pulmonary artery disease, contrast-enhanced computed tomographic angiography (CE-CTA) represents the standard clinical reference method for diagnosing

APE [3–7]. In the PIOPED II study, CE-CTA achieved a sensitivity of 83% and a specificity of 96% [3]. Due to technical innovations such as dual energy CT, more recent studies have reported even better results for CE-CTA [8, 9].

APE is usually detected using CE-CTA in emergency settings and departments. CE-CTA is associated with intrinsic disadvantages, however, including radiation exposure, which is associated with higher cancer risks, and the need for iodinated contrast agents. Therefore, inappropriate use of CE-CTA raises concerns particularly in young and pregnant patients as well as in patients suffering from chronic kidney disease [10].

Magnetic resonance angiography using gadolinium-based contrast agent (CE-MRA) represents an alternative diagnostic technique for APE with fewer drawbacks than CE-CTA [11]. The multi-center PIOPED III study reported a sensitivity of 78% and a specificity of 99% for pulmonary embolism, but included the limitation that 25% of the evaluated patients had been excluded previously due to technically inadequate CE-MRA examinations [5]. Another study showed that a negative predictive value of 97% for excluding APE could be achieved by means of CE-MRA [12].

Side effects of gadolinium-based contrast agents (GBCA) such as nephrogenic systemic fibrosis and cerebral gadolinium deposits have been reduced in recent studies with the use of more stable, macrocyclic GBCA [13]. Nevertheless, the use of non-CE MRA techniques for the diagnosis of APE is desirable.

In addition to reasonable concerns about the safety of both iodinated and gadolinium-based contrast agents, the requirement for breath-holding during standard CE-MRA pulse sequences has driven new developments in non-CE imaging methods of pulmonary embolism [14].

The balanced steady-state free precession (bSSFP) pulse sequence is a non-CE single-shot magnetic resonance imaging (MRI) technique by which intravascular clots can be visualized during free-breathing [11, 15]. Here, bSSFP imaging is normally applied using a Cartesian k-space sampling trajectory and without cardiac gating. However, images of the central pulmonary arteries are blurry due to pulsation of the thoracic vessels over the cardiac cycle [16, 17]. In addition, the sensitivity of Cartesian bSSFP for APE decreases in more distal branches of the pulmonary arteries due to respiratory motion effects [18].

Edelman et al. recently introduced a respiratory navigator-gated and electrocardiographic (ECG) gated implementation of radial quiescent-interval slice-selective (QISS) for non-CE MRA of the pulmonary arteries in patients with suspected pulmonary embolism in free-breathing [19]. Radial k-space trajectories provide several potential advantages over Cartesian trajectories, including reduced motion sensitivity and higher temporal and spatial resolution [20, 21]. Although the use of ECG gating can extend the duration of an MRA examination, it provides high arterial signal intensity, reduces arterial pulsation artifacts, and more reliably distinguishes of intravascular clots from surrounding tissue.

The aim of this study was to investigate the clinical performance of free-breathing non-navigator-gated and ECG gated radial QISS-MRA for the diagnosis of APE compared to CE-CTA as the standard clinical technique and to non-CE Cartesian bSSFP-MRA.

Material and Methods

The local institutional review board approved this prospective single-center study (No. D 508/18). All study participants gave their informed consent in written form.

Patients

From January to October 2019, a total of 4370 patients were consecutively referred to our university medical center for thoracic CE-CTA imaging. An APE was detected in 236 of these 4370 patients (5.4%). Patients in unstable cardiopulmonary condition or with severe pulmonary artery thrombus load requiring to transfer to the intensive care unit, with a history of pulmonary surgery, with a cardiac pacemaker, large-sized ferromagnetic materials in the thoracic region, or further contraindications for MRI were excluded from our study. Within 24 hours after the CE-CTA examination, MRA images were acquired in 30 of 236 patients (12.7%) who had received appropriate anticoagulation (direct oral anticoagulants (DOACs) in 14 patients, low-molecular-weight heparins (LMWHs) in 15 patients, phenprocoumon in combination with LMWH in one patient) to prevent progression of APE with life-threatening complications, such as right ventricular failure. The median time interval between CE-CTA and both MRA examinations was 9 hours and 51 minutes with an interquartile range of 3 hours and 38 minutes to 16 hours and 42 minutes hours and a minimum to maximum range of 1 hour and 2 minutes to 23 hours and 39 minutes.

Healthy volunteers

As a control group, 30 healthy volunteers (HVs) were included in this study to methodologically compare the two MRA techniques (Table 1). The status “healthy” was based on the following criteria: 1) absence of acute or chronic pulmonary artery embolism or pulmonary artery hypertension in the medical history, and 2) no history of inflammatory, malignant, or fibrotic lung disease or pulmonary artery stenosis before the examination. The general exclusion criteria for MRI safety were identical to those of the patient group.

Demographic data of study population

Pertinent demographics (age, weight, body mass index at examination, and gender) of the study population are included in Table 1.

Non-CE MRA

Imaging was performed on a 1.5-Tesla MRI system (Magnetom Aera, XQ gradients, syngo MR VE11C software, Siemens Healthcare GmbH, Erlangen, Germany) with a maximum gradient of 45 mT/m and a maximum slew rate of 200 T/m/s. The MRI signal was received using a combination of an 18-element torso coil with a 32-element spine array coil from the same manufacturer. The clinical non-CE MRA reference technique of Cartesian bSSFP-MRA was performed first [22], which was followed by radial QISS-MRA [19, 21]. This order remained the same for all examinations in both patients and HVs. Imaging with both

pulse sequences was performed in transversal, coronal, and sagittal slice orientations under free-breathing conditions with the parameters shown in supplementary Table S1.

CE-CTA

Thoracic CE-CTA images were acquired using four CT systems with the available protocol parameters presented in supplementary Table S2.

Image analysis

Initial diagnosis of APE was made by a board-certified radiologist based on CE-CTA. After including 30 patients in our study, APE in these CE-CTA datasets was graded by a consensus decision of two radiologists (K. T. and A. L.), each with at least 5 years of experience interpreting pulmonary CTA and MRA images. Subsequently, a total of 120 MRA datasets (patients and HVs: 30 radial QISS-MRA and 30 Cartesian bSSFP-MRA datasets, respectively) were evaluated by the two radiologists (K. T. and A. L.) independently during separate sessions. For calculating intraobserver agreement, the two radiologists independently analyzed the 60 MRA datasets obtained in the patients twice in separate sessions. The time interval between the first and second analysis of each radiologist was at least two months. In total, 150 datasets were included in our study and each radiologist conducted a total of 210 analyses. Image analysis was performed on a workstation (IMPAX EE, Agfa HealthCare GmbH, Bonn, Germany).

MRA datasets were analyzed from both a technical and a clinical perspective. The two radiologists (K. T. and A. L.) rated the technical quality of MRA images independently using a scoring scale of 0 (no artifact) to 1 (artifact present) with respect to various imaging artifacts (Figure 1). If an artifact was found, it was classified as either 1a, 1b, 1c, or 1d as follows:

Grade 0: Absence of imaging artifacts

Grade 1: Presence of

- **a.** imperfect steady-state artifacts (for Cartesian readout in bSSFP-MRA) based on magnetic field inhomogeneity, pulsation of pulmonary arteries, and blood flow turbulence in the pulmonary arteries and in the ascending aorta
- **b.** streaking artifacts (for radial readout in QISS-MRA)
- **c.** breathing artifacts
- **d.** thrombus-mimicking artifacts based on blood flow turbulence

Specific image artifacts (a or b) were assigned for only one of the MRA methods (radial QISS-MRA or Cartesian-MRA), whereas general image artifacts (c or d) were assigned for both MRA methods.

The pulmonary arterial tree was anatomically divided into four sections: central arteries (main pulmonary artery, right and left pulmonary artery), lobar branches (right and left side), segmental branches and subsegmental branches. However, we evaluated segmental and subsegmental branches together as peripheral regions due to the great variation in the

subsegmental pulmonary arterial pattern [23, 24]. For assessing diagnostic quality, the pulmonary arterial tree was divided into 25 branches according to the Boyden classification of bronchi [25]. The superior and inferior lingular segments were evaluated as one segment.

The pulmonary artery branches were evaluated based on assessment of continuity, visibility, and edge sharpness by using an image quality scoring scale of 1 to 4:

Grade 1: Nondiagnostic, barely visible lumen or nondemarcated pulmonary branch

Grade 2: Fair, ill-defined vessel borders with suboptimal image quality for diagnosis

Grade 3: Good, minor inhomogeneities not influencing vessel delineation

Grade 4: Excellent, sharply defined arterial borders with excellent image quality for highly confident diagnosis

The presence or absence of pulmonary embolism was evaluated in all three slice orientations. As reliable assessment of the pulmonary embolism depends on the shape and orientation of a visualized vessel in a certain slice orientation, the final decision concerning the presence or absence of PE was based on the slice orientation data that most clearly showed the arterial segment under evaluation. PE was graded based on the final decision using a scoring scale of 0 to 2:

Grade 0: No thrombus in the pulmonary artery.

Grade 1: Presence of thrombus with remaining perfusion of the pulmonary artery.

Grade 2: Total occlusion of the pulmonary artery.

In addition, we also analyzed whether the diagnostic accuracy of APE was affected by the imaging slice orientation.

The signal-to-noise ratio (SNR) and contrast-to-noise ratio (CNR) were computed to compare pulmonary MRA imaging quality between the two MRA methods. Three regions of interest (ROIs) with the same area (200 mm^2) were placed in the middle of the pulmonary trunk ($ROI_{Pulmonary\ trunk}$, 1.0 cm ventral from the bifurcation), in the background without any visual imaging artifacts (ROI_{Air}), and in the pulmonary tissue of the lingual segment in a region without large vessels and without image artifacts (ROI_{Lung}). The SNR and CNR were determined using the extracted mean value and standard deviation (sd) of the signal intensities (SI) from these ROIs as follows [26]:

$$SNR = 0.655 \cdot \frac{mean\ (SI_{Pulmonaly\ trunk})}{sd\ (SI_{Air})}, CNR = 0.655 \cdot \frac{mean\ (SI_{Pulmonaly\ trunk} - SI_{Lung})}{sd\ (SI_{Air})}$$

Statistical analysis

Normality (Gaussian distribution) was tested for all variables using the Shapiro–Wilk test. Median and range of variables were reported as summary statistics for all variables due to the severe skewness of the respective distributions. The p-values for comparison of two groups were obtained from a Wilcoxon signed-rank test. All significant p-values were reported with a precision of 10^{-5}. A p-value <0.05 was considered statistically significant.

All three angiographic methods for APE grading were correlated using the Spearman's correlation test [27]. The strength of the Spearman's correlation was defined as perfect (r=1.0), very strong (1.0>r≥0.80), moderate (0.80>r≥0.60), fair (0.60>r≥0.30), and poor (r<0.30) [28]. CE-CTA was used as a clinical reference method for determining diagnostic performance of the two MRA techniques using a dedicated statistical software package (Module diagnostic test, MedCalc, Version 2019, MedCalc bvba, Ostend, Belgium). These values were presented with exact 95% confidence intervals (CI) derived from the binomial distribution. To determine diagnostic performance of the MRA methods, the APE grading results of the two radiologists were considered together as one group (750 pulmonary branches x 2 radiologists = 1500 pulmonary branches). Moreover, positive APE findings (grades 1 and 2) were considered as one group versus negative findings (grade 0). The APE grades were not compared. Intra- and interobserver agreement on the scoring of an image was assessed by quadratic, weighted concordance [29]. Concordance was calculated with the rater's package (CRAN: raters). Agreement was interpreted as follows: <0.00, poor agreement; 0.00-0.20, slight agreement; 0.21-0.40, fair agreement; 0.41-0.60, moderate agreement; 0.61-0.80, substantial agreement; 0.81-1.00, or almost perfect agreement [30]. The correlation and concordance values were determined using the R Statistic package (version 3.5.1, R Foundation for Statistical Computing, Vienna, Austria). Diagrams were plotted with MATLAB (Version 2017a, The MathWorks, Natick, MA, USA).

Results

Characteristics of study population

Relevant data for the study population are summarized in Table 1.

SNR and CNR

The relative increase in SNR provided by radial QISS-MRA with respect to Cartesian bSSFP was 29.6% in HVs and 33.8% in patients. The relative increase in CNR provided by radial QISS-MRA with respect to Cartesian in HVs and in patients was in line with the SNR results (HVs: 31.3%, patients: 35.7%) (Tables 2 and 3).

Presence of specific and general imaging artifacts

Imperfect steady-state artifacts were observed in all three slice directions of Cartesian bSSFP-MRA and occurred mainly in the central and lobar branches in both the HV and patient cohorts (HVs/Patients: pulmonary trunk vs. lobar arteries: p<0.0001/p<0.0001; pulmonary trunk vs. peripheral arteries: p<0.0001/p<0.0001; lobar vs. peripheral arteries: p<0.0001/p<0.0001. HVs vs. patients: pulmonary trunk: p=1, lobar arteries: p=0.003, peripheral arteries: p<0.0001, Figures 2a and 3a).

Streaking artifacts occurred in all three slice directions of radial QISS-MRA in all three pulmonary regions, especially in the transversal slice orientation (HVs/Patients: pulmonary trunk vs. lobar arteries: p=0.005/p<0.0001; pulmonary trunk vs. peripheral arteries: p=0.001/p=0.01; lobar vs. peripheral arteries: p<0.0001/p<0.0001. HVs vs. patients: pulmonary trunk: p<0.0001, lobar arteries: p<0.0001, peripheral arteries: p<0.0001. In HVs, transversal vs. coronal/transversal vs. sagittal, pulmonary trunk: p<0.0001/p<0.0001, lobar arteries:

p<0.0001/p<0.0001, peripheral arteries: p=0.0005/p=0.0005. In patients, transversal vs. coronal/transversal vs. sagittal, pulmonary trunk: p=0.11/p=0.003, lobar arteries: p=0.02/p=0.26, peripheral arteries: p=0.57/p=0.30, Figures 2b and 3b).

Regardless of the slice orientation, breathing artifacts more frequently appeared in HVs with Cartesian bSSFP-MRA (radial QISS-MRA vs. Cartesian bSSFP-MRA, pulmonary trunk: p=0.02, lobar arteries: p<0.0001, peripheral arteries: p<0.0001, Figure 2c). In patients, no significant differences were observed between radial QISS-MRA and Cartesian bSSFP-MRA regarding breathing artifacts (radial QISS-MRA vs. Cartesian bSSFP-MRA, pulmonary trunk: p=0.06, lobar arteries: p=0.59, peripheral arteries: p=0.31, Figure 3c). Breathing artifacts with radial QISS-MRA were more frequently found in patients than in HVs (HVs vs. patients: pulmonary trunk: p=0.01, lobar arteries: p<0.0001, peripheral arteries: p<0.0001). In contrast, these artifacts occurred with a similar frequency in both HVs and patients with Cartesian bSSFP-MRA, apart from lobar arteries (HVs vs. patients: pulmonary trunk: p=0.10, lobar arteries: p=0.004, peripheral arteries: p=0.76).

Thrombus-mimicking artifacts in HVs appeared more frequently with Cartesian bSSFP-MRA than with radial QISS-MRA (radial QISS-MRA vs. Cartesian bSSFP-MRA, pulmonary trunk: p<0.0001, lobar arteries: p<0.0001, peripheral arteries: p<0.0001, Figure 2d). These artifacts were more commonly observed in patients, predominantly in lobar and peripheral arteries, with Cartesian bSSFP-MRA than with radial QISS-MRA (radial QISS-MRA vs. Cartesian bSSFP-MRA, pulmonary trunk: p=0.64, lobar arteries: p=0.005, peripheral arteries: p<0.0001, Figure 3d). With radial QISS-MRA, thrombus-mimicking artifacts occurred significantly more frequently in patients than in HVs (HVs vs. patients: pulmonary trunk: p<0.0001, lobar arteries: p=0.04, peripheral arteries: p<0.0001), while a significant difference between HVs and patients appeared only in lobar arteries with Cartesian bSSFP-MRA (HVs vs. patients: pulmonary trunk: p=0.74, lobar arteries: p=0.01, peripheral arteries: p=0.90).

Image quality of pulmonary arterial segments

Clinically, a total of 5250 arterial branches (25 arterial branches from each of 210 analyses) were assessed.

Each radiologist (K. T. and A. L.) independently evaluated 750 pulmonary branches (30 subjects × 25 pulmonary branches) in both HVs and patients, respectively. For statistical analysis, the evaluation results of the two radiologists were considered together as one group (750 pulmonary branches x 2 radiologist = 1500 pulmonary branches). This approach was used for the visualization of pulmonary branches as well as for the assessment of APE grading.

Healthy Volunteers: For radial QISS-MRA, the readers together scored 46.6% (699/1500) of branches as grade 4 (excellent), 47.8% (717/1500) as grade 3 (good), 5.5% (82/1500) as grade 2 (fair), and 0.1% (2/1500) as grade 1 (non-diagnostic). For Cartesian bSSFP-MRA, the readers together identified 3.8% (57/1500) of branches as grade 4, 67.7% (1015/1500) as grade 3, 27.2% as grade 2 (408/1500), and 1.3% (20/1500) as grade 1. The image quality of pulmonary arterial branches was considered diagnostically as “good to

excellent, grade≥3" in 94.4% (1416/1500) with radial QISS-MRA and in 71.5% (1072/1500) with Cartesian bSSFP-MRA (p<0.0001). Compared to Cartesian bSSFP-MRA, radial QISS-MRA provided significantly improved image quality in 23 of 25 pulmonary branches (Table 2).

Patients: For radial QISS-MRA, the readers together scored 28.0% (420/1500) of branches as grade 4, 49.2% (738/1500) as grade 3, 20.0% as grade 2 (300/1500), and 2.8% (42/1500) as grade 1. For Cartesian bSSFP-MRA, the readers together identified 0.0% (0/1500) of branches as grade 4, 43.2% (648/1500) as grade 3, 51.9% as grade 2 (779/1500), and 4.9% (73/1500) as grade 1.The image quality of pulmonary arterial branches was considered diagnostically as "good to excellent, grade≥3" in 77.2% (1158/1500) with radial QISS-MRA and in 43.2% (648/1500) with Cartesian bSSFP-MRA (p<0.0001). Radial QISS-MRA provided significantly better image quality than Cartesian bSSFP-MRA in all pulmonary regions (Table 3, Figure 4).

Pulmonary artery embolism

The correlation between the two MRA methods and CE-CTA, and also between the two MRA methods themselves was based on accurate determination of APE grading (Grades 0, 1 and 2) in all pulmonary branches of patients. In order to compare our results with data in the literature, the results of branches were stratified into three pulmonary regions (central, lobar, and peripheral arteries) in Table 4. Concerning the CE-CTA, radial QISS-MRA provided a very strong correlation in all three pulmonary regions (0.82 – 0.88), while Cartesian bSSFP-MRA only correlated moderately in corresponding regions (0.67 – 0.74). A decreased correlation from central to peripheral arterial region could be observed between the two MRA methods and between CE-CTA and each MRA method.

An accurate APE (all grades) could be determined in 90.1% of cases with radial QISS and in 82.4% with Cartesian bSSFP. The degree of APE was underestimated in 5.7% of cases with radial QISS and in 9.4% with Cartesian bSSFP. An overestimation of APE was observed in 4.2% of cases with radial QISS and in 8.2% with Cartesian bSSFP (Table S3).

A per-patient analysis revealed a minimum of 1 to a maximum of 24 pulmonary branches with arterial embolism in CE-CTA. This range was also detected using both MRA methods. There were no significant differences between the number of pulmonary branches with arterial embolism detected using CE-CTA (median [interquartile range], 9.5 [5, 15]), radial QISS-MRA (9.5 [4, 15]), and Cartesian bSSFP (9.5 [3, 16]). CE-CTA vs. radial QISS-MRA: p=0.76; CE-CTA vs. Cartesian bSSFP-MRA: p=0.83, radial QISS-MRA vs. Cartesian bSSFP-MRA: p=0.89.

Impact of imaging slice orientation on accurate detection of APE

In patients, the results of both observers for each MRA method were compared to the CE-CTA findings for three slice orientations. There was a strong correlation between findings of CE-CTA and radial QISS-MRA (r-value of transversal/coronal/sagittal: 0.85/0.84/0.83 with a p<0.0001 for all directions) and a moderate correlation between CE-CTA and Cartesian

bSSFP-MRA (r-value of transversal/coronal/sagittal: 0.70/0.70/0.70 with a $p<0.0001$ for all directions).

Clinical performance of QISS-MRA

Radial QISS-MRA provided a total sensitivity of 86.0%, a specificity of 93.4%, and an accuracy of 90.4% for diagnosis of APE using CE-CTA as clinical reference standard. These values were up to 8% lower in Cartesian bSSFP-MRA (Table 5). In addition to three pulmonary regions (central, lobar, and peripheral arteries), the grading results of all 1500 pulmonary arterial branches were summarized for each MRA technique to simplify the comparison between the two MRA methods regarding CE-CTA.

Intra- and interobserver agreement

A substantial to almost perfect interobserver and intraobserver agreement was found for image quality scoring of anatomical segments and for the diagnosis of APE in patients with both MRA methods (Table 6).

Discussion

Free-breathing non-CE MRA techniques are of considerable interest for diagnosing APE owing to their high accuracy in visualizing clots in the pulmonary arteries [31], the possibility for repeated examinations, and the avoidance of possible side effects of administering GBCAs and radiation exposure compared to CE-CTA.

In the literature [32], some non-CE MRA techniques, such as 2D/3D time-of-flight (TOF), 3D fast spin echo (FSE), fresh blood imaging (FBI), arterial spin labeling (ASL), and Cartesian bSSFP [33] have been introduced for visualizing pulmonary arteries. Apart from Cartesian bSSFP, none of the other pulse sequences could be successfully implemented in clinical routine due to the limited anatomical coverage, dependency on the patient's breath-holding capability, registration artifacts between tagged and untagged images, poor image quality, and subsequent poor visualization of thrombus [31, 32, 34].

In our prospective study, radial QISS-MRA was evaluated from technical and clinical points of view in patients with confirmed APE and in HVs compared to Cartesian bSSFP-MRA and CE-CTA. In addition, the clinical performance of both MRA methods for diagnosing APE was investigated using CE-CTA as clinical reference method.

Our study found that: 1) radial QISS-MRA provided higher SNR and CNR than Cartesian bSSFP-MRA; 2) thrombus-mimicking artifact appeared more frequently with Cartesian bSSFP-MRA than with radial QISS-MRA; 3) radial QISS-MRA provided superior image quality in comparison with Cartesian bSSFP-MRA; 4) there was a higher correlation between radial QISS-MRA and CE-CTA than for Cartesian bSSFP-MRA concerning the accurate diagnosis of APE grading; and 5) based on detailed segmental evaluation by two experienced radiologists, radial QISS-MRA provided a higher sensitivity, specificity, and accuracy than Cartesian bSSFP-MRA for detecting APE using CE-CTA as the clinical reference method.

Technical aspects:

In the present work, the prevalence of four distinct image artifacts during radial QISS-MRA and Cartesian bSSFP-MRA were analyzed for three anatomical pulmonary regions (central, lobar and peripheral arteries) and when imaging was performed using three slice orientations (transversal, coronal, and sagittal).

Imperfect steady-state artifacts occurred only with Cartesian bSSFP-MRA due to the greater sensitivity of Cartesian k-space sampling to flow through B_0-magnetic field inhomogeneity, and to pulsation of pulmonary arteries and ascending aorta. Data acquisition using ECG gating and radial k-space trajectory eliminated these artifacts [35]. In addition, data acquisition during diastole improved SNR and CNR in the pulmonary arteries and better differentiated the arteries from the surrounding pulmonary tissue.

The radial k-space trajectory used in this study was undersampled with respect to the Nyquist sampling rate. This approach is beneficial as it accelerates data acquisition, which means that this technique will be less susceptible to cardiac motion and to the pulsation of pulmonary arteries than Cartesian sampling (e.g. bSSFP-MRA). However, undersampled radial MRI data are prone to streaking artifacts. The appearance and strength of these artifacts depend on the number of acquired radial projections. In our work, for which 150 radial projections were acquired, streaking artifacts were observed mostly in the transversal slice direction of all three pulmonary regions (pulmonary trunk, lobar, and peripheral arteries) in both HVs and patients. While such artifacts were regularly noted with radial QISS-MRA in the periphery of the field of view, they were not often found to materially degrade the image quality of the pulmonary arteries. Such artifacts can be reduced by increasing the number of acquired radial projections, but imaging would likely extend into the next cardiac cycle and lengthen measurement time. The implementation of radial QISS-MRA used in our study did not include any acceleration technique, such as parallel imaging or compressed sensing [36]. Incorporating one of these acceleration techniques with radial QISS-MRA may help to reduce streaking-artifacts and shorten measurement time.

Breathing artifacts of thoracic CT and MR images can be reduced using breath-holding techniques. Data acquisition during inspiration is more convenient for most patients than during expiration. However, patients with APE frequently have a limited capacity for breath-holding during data acquisition. Moreover, image acquisition during inspiration leads to changes in pulmonary blood flow and further increases the initially embolism-related pulmonary pressure and arterial resistance [37]. We therefore evaluated the performance of both MRA techniques under free-breathing conditions.

In HVs, the acquired thoracic datasets using Cartesian bSSFP-MRA were strongly affected by breathing artifacts, especially in the region of lobar and peripheral arteries. Conversely, these artifacts were reduced significantly with radial QISS-MRA in the peripheral arteries and occurred only infrequently in the lobar arteries.

In comparison with data obtained in HVs, patient images with radial QISS-MRA were significantly affected by breathing artifacts in all pulmonary regions. Thus, radial QISS-MRA was shown to be more sensitive than Cartesian QISS-MRA to irregular breathing

movement of patients during a measurement. Two potential strategies for reducing breathing artifacts during free-breathing radial QISS-MR might include: 1) acquiring the data more rapidly in patients than in HVs (<1 sec per slice) or 2) applying respiratory gating to limit data acquisition to a particular phase of the respiratory cycle [38].

Thrombus-mimicking artifact is another imaging artifact that can hamper the diagnostic utility of CE- or non-CE MRA of the pulmonary arteries. Apart from the transversal slice orientation of the pulmonary trunk, Cartesian bSSFP-MRA was significantly more susceptible to thrombus-mimicking artifacts than radial QISS-MRA in all pulmonary arterial regions and slice orientations. These artifacts were observed more frequently in the lobar and peripheral arteries than in the central region of Cartesian bSSFP-MRA as compared to radial QISS-MRA. Moreover, these artifacts appeared more commonly on transverse images and near the branching of arteries. Thrombus-mimicking artifacts can be reduced by turning off the in-plane saturation of the QISS-MRA pulse sequence (to not suppress in-plane flow), using radial rather than Cartesian sampling, and possibly by applying additional measures for flow compensation during bSSFP imaging [39].

Clinical aspects:

For the first part of our clinical evaluation, all 25 pulmonary arterial branches were analyzed in HVs and patients. The detailed analysis of the image quality of arterial branches in our study population revealed that radial QISS-MRA provides excellent visualization of all arterial vessels with various shapes, lengths, and diameters. Herédia et al. [40] evaluated the visualization of pulmonary arteries in three regions (central, lobar, and segmental) and Edelman et al. [19] in 25 branches. The results of the quality of arterial visualization with both MRA techniques in our present work are in good agreement with both of these studies.

The second part of our clinical evaluation was focused on the comparison between the CE-CTA findings and those of both MRA techniques in patients for diagnosing three grades of APE in all pulmonary arterial branches. Our results showed a very strong correlation between radial QISS-MRA and CE-CTA, and a moderate correlation between Cartesian bSSFP-MRA and CE-CTA. Both MRA methods were performed in a median time interval of 9 hours and 51 minutes hours after the CE-CTA examination and after anticoagulation therapy. The thrombus mass could have changed after anticoagulation. The literature on the rate of clot resolution after anticoagulation in patients with APE is limited. However, based on the follow-up CT data presented by Choi et al. [41], the rate of complete resolution of pulmonary emboli is 24% at 3-4 days, 47% at 8-21 days, and 78% at 22-90 days. Consequently, it is unlikely that pulmonary embolism resolved within 24 hours. This negligible degree of pulmonary embolism resolution therefore would have likely only minimally influenced the comparison between our MRA methods and CE-CTA. Furthermore, both MRA methods were performed in the same session. Therefore, a possible slight change in the mass of the embolism would have influenced the two MRA techniques similarly.

In the third step of our clinical evaluation, we investigated the impact of imaging slice orientation for detecting APE. This issue is important for constructing time-efficient non-CE MRA protocols for use, in particular, in cases of emergency without loss of diagnostic

accuracy. Comparison between the CE-CTA findings and those of the two MRA techniques indicated that all three slice directions are equally accurate in diagnosing APE. Hosch el. al. [42] investigated the clinical performance of real-time bSSFP-MRA in three separate slice orientations (transversal, coronal, and sagittal) and in combination for diagnosing acute central and lobar pulmonary embolism. They reported a higher sensitivity of 90% and a specificity of 94% for the transversal view. The corresponding values of coronal and sagittal views were up to 9% lower than those of the axial view. A combination of all three views provided a slightly higher sensitivity of 93% and specificity of 95%. The transversal plane is usually an important slice direction from the radiological point of view for diagnosis based on thoracic MRA data. According to the data of Hosch et. al., an additional anatomical view (coronal or sagittal) could improve the diagnosis, but only to a negligible degree. Future work might consider investigating 3D MRA methods to reduce measurement time and improve the diagnosis of APE.

In the fourth part of our clinical evaluation, we analyzed clinical performance of the two MRA techniques compared to CE-CTA findings in all patients. Radial QISS-MRA provided a higher sensitivity, specificity, positive/negative predictive value, and accuracy than Cartesian bSSFP-MRA. In several previous publications, the clinical performance of Cartesian bSSFP-MRA was evaluated compared to CE-CTA in two, three or four pulmonary regions (central, lobar, segmental, and subsegmental) [11, 18, 42–44]. Some of these publications included a homogeneous patient group with APE and some included a mixture of patients in whom APE was clinically suspected and in those with confirmed APE based on CE-CTA findings. There is no comparable publication for evaluating the clinical performance of radial QISS-MRA.

In a study involving 22 patients, Kalb et al. [43] found that Cartesian bSSFP-MRA provided a sensitivity of 67% and a specificity of 100%. In another study [18], in which inconclusive MRI data were excluded, the sensitivity of Cartesian bSSFP-MRA ranged from 70% to 72% and the specificity from 84.5% to 99.1%. Hosch et al. [42] reported a sensitivity of 93%, a specificity of 95%, and a positive/negative predictive value of 94%/90% for diagnosing central and lobar APE only using real-time Cartesian bSSFP. In 91 patients in whom APE was clinically suspected, Pasin et al. [11] performed a per-embolus analysis for Cartesian bSSFP-MRA in pulmonary trunk, lobar, segmental, and subsegmental arteries. The PE was confirmed in 20 of their patients (22%). They presented a total sensitivity of 85%, a specificity of 95.8%, and an accuracy of 94.5%. Kaya et al. [44] evaluated the clinical performance of Cartesian bSSFP-MRA for diagnosing PE in lobar and segmental regions of 44 patients compared to CE-CTA. In the lobar regions, they reported a sensitivity of 67.9%, a specificity of 99.7%, and an accuracy of 91.6%. The corresponding values in segmental regions were 2-39% lower than those in the lobar region.

All 30 patients in our study had a confirmed APE based on the CE-CTA findings. Taking into account different study protocols, our results concerning Cartesian bSSFP-MRA are similar to previously published data. This corroborates our findings in general, including the superior performance of radial QISS-MRA compared to Cartesian bSSFP-MRA.

Analysis of intra- and interobserver agreement of image quality scores of all pulmonary arterial regions and the diagnosis of APE in the last part of our clinical evaluation showed substantial to almost perfect agreements for both MRA methods. Our results for Cartesian bSSFP-MRA are in good agreement with those in the literature [11, 18, 43].

Limitations of the study

Our study was focused on a detailed analysis of 25 pulmonary arterial branches and the grading of occlusions. Therefore, only patients with confirmed APE were included in our study. Nevertheless, more than one branch was correctly identified as positive for APE in 29 of 30 patients by both MRA methods. Thus, on a per-patient basis, the clinical diagnosis of APE could be reliably confirmed. The patients and HVs were analyzed separately and not as one group in order to investigate the influence of clinical epiphenomena of patients, such as tachycardia and reduced breathing capacities on the image quality and accurate diagnosis of APE.

Conclusions

This study indicates that free-breathing non-navigator-gated and ECG gated radial QISS-MRA is a reliable angiographic technique with promising clinical potential for portraying the pulmonary arteries and detecting APE. Radial QISS-MRA is a feasible alternative to CE-CTA without radiation exposure for patients with contraindications to iodine-based contrast agents, especially in high-risk patients with renal impairment, or young or pregnant patients. Furthermore, with respect to Cartesian bSSFP-MRA, radial QISS-MRA improved image quality.

Supplementary Material

Refer to Web version on PubMed Central for supplementary material.

Acknowledgments:

The authors would like to thank all healthy volunteers and patients for participating in our study. We thank our technicians for their assistance in MRA examinations. We warmly thank our colleagues from the Department of internal Medicine I, II, and III, from the Department of Surgery, from the Department of Radiotherapy, from the Department of Neurology, from the Department of Neurosurgery, and from the Department of Urology for their assistance in patient management.

Grant Support

This work was supported in part by the National Institutes of Health under award numbers R01HL137920 and R01EB027475. The content is solely the responsibility of the authors and does not necessarily represent the official views of the National Institutes of Health.

References

1. Islam M, Filopei J, Frank M, Ramesh N, Verzosa S, Ehrlich M, et al. Pulmonary infarction secondary to pulmonary embolism: An evolving paradigm. Respirology. 2018.
2. Simcox LE, Ormesher L, Tower C, Greer IA. Pulmonary thrombo-embolism in pregnancy: diagnosis and management. Breathe (Sheff). 2015;11:282–9. [PubMed: 27066121]

3. Stein PD, Fowler SE, Goodman LR, Gottschalk A, Hales CA, Hull RD, et al. Multidetector computed tomography for acute pulmonary embolism. N Engl J Med. 2006;354:2317–27. [PubMed: 16738268]
4. Benson DG, Schiebler ML, Repplinger MD, Francois CJ, Grist TM, Reeder SB, Nagle SK. Contrast-enhanced pulmonary MRA for the primary diagnosis of pulmonary embolism: current state of the art and future directions. Br J Radiol. 2017;90:20160901. [PubMed: 28306332]
5. Stein PD, Chenevert TL, Fowler SE, Goodman LR, Gottschalk A, Hales CA, et al. Gadolinium-enhanced magnetic resonance angiography for pulmonary embolism: a multicenter prospective study (PIOPED III). Ann Intern Med. 2010;152:434–43, W142–3. [PubMed: 20368649]
6. Stein PD, Gottschalk A, Sostman HD, Chenevert TL, Fowler SE, Goodman LR, et al. Methods of Prospective Investigation of Pulmonary Embolism Diagnosis III (PIOPED III). Semin Nucl Med. 2008;38:462–70. [PubMed: 19331840]
7. Ruggiero A, Screaton NJ. Imaging of acute and chronic thromboembolic disease: state of the art. Clin Radiol. 2017;72:375–88. [PubMed: 28330686]
8. Grob D, Smit E, Prince J, Kist J, Stoger L, Geurts B, et al. Iodine Maps from Subtraction CT or Dual-Energy CT to Detect Pulmonary Emboli with CT Angiography: A Multiple-Observer Study. Radiology. 2019;292:197–205. [PubMed: 31084482]
9. Abdellatif W, Ebada MA, Alkanj S, Negida A, Murray N, Khosa F, Nicolaou S. Diagnostic Accuracy of Dual-Energy CT in Detection of Acute Pulmonary Embolism: A Systematic Review and Meta-Analysis. Can Assoc Radiol J. 2020:846537120902062.
10. Smith-Bindman R, Lipson J, Marcus R, Kim K-P, Mahesh M, Gould R, et al. Radiation dose associated with common computed tomography examinations and the associated lifetime attributable risk of cancer. Arch Intern Med. 2009;169:2078–86. [PubMed: 20008690]
11. Pasin L, Zanon M, Moreira J, Moreira AL, Watte G, Marchiori E, Hochhegger B. Magnetic Resonance Imaging of Pulmonary Embolism: Diagnostic Accuracy of Unenhanced MR and Influence in Mortality Rates. Lung. 2017;195:193–9. [PubMed: 28116500]
12. Schiebler ML, Nagle SK, Francois CJ, Repplinger MD, Hamedani AG, Vigen KK, et al. Effectiveness of MR angiography for the primary diagnosis of acute pulmonary embolism: clinical outcomes at 3 months and 1 year. J Magn Reson Imaging. 2013;38:914–25. [PubMed: 23553735]
13. Radbruch A, Richter H, Fingerhut S, Martin LF, Xia A, Henze N, et al. Gadolinium Deposition in the Brain in a Large Animal Model: Comparison of Linear and Macrocyclic Gadolinium-Based Contrast Agents. Invest Radiol. 2019;54:531–6. [PubMed: 31261291]
14. Tsuchiya N, van Beek E JR, Ohno Y, Hatabu H, Kauczor H-U, Swift A, et al. Magnetic resonance angiography for the primary diagnosis of pulmonary embolism: A review from the international workshop for pulmonary functional imaging. World J Radiol. 2018;10:52–64. [PubMed: 29988845]
15. Ley S Imaging pulmonary arterial thromboembolism: challenges and opportunities. Magn Reson Imaging Clin N Am. 2015;23:261–71. [PubMed: 25952519]
16. Reimer P, Parizel PM, Meaney JFM, Stichnoth FA. Clinical MR Imaging: A Practical Approach: Springer Berlin Heidelberg; 2010.
17. Saremi F, Grizzard JD, Kim RJ. Optimizing cardiac MR imaging: practical remedies for artifacts. Radiographics. 2008;28:1161–87. [PubMed: 18635635]
18. Revel MP, Sanchez O, Lefort C, Meyer G, Couchon S, Hernigou A, et al. Diagnostic accuracy of unenhanced, contrast-enhanced perfusion and angiographic MRI sequences for pulmonary embolism diagnosis: results of independent sequence readings. Eur Radiol. 2013;23:2374–82. [PubMed: 23652845]
19. Edelman RR, Silvers RI, Thakrar KH, Metzl MD, Nazari J, Giri S, Koktzoglou I. Nonenhanced MR angiography of the pulmonary arteries using single-shot radial quiescent-interval slice-selective (QISS): a technical feasibility study. J Cardiovasc Magn Reson. 2017;19:48. [PubMed: 28662717]
20. Glover GH, Pauly JM. Projection reconstruction techniques for reduction of motion effects in MRI. Magn Reson Med. 1992;28:275–89. [PubMed: 1461126]

21. Edelman RR, Botelho M, Pursnani A, Giri S, Koktzoglou I. Improved dark blood imaging of the heart using radial balanced steady-state free precession. J Cardiovasc Magn Reson. 2016;18:69. [PubMed: 27756330]
22. Bieri O, Scheffler K. Fundamentals of balanced steady state free precession MRI. J Magn Reson Imaging. 2013;38:2–11. [PubMed: 23633246]
23. CORY RA, VALENTINE EJ. Varying patterns of the lobar branches of the pulmonary artery. A study of 524 lungs and lobes seen at operation of 426 patients. Thorax. 1959;14:267–80. [PubMed: 13812149]
24. Kandathil A, Chamarthy M. Pulmonary vascular anatomy & anatomical variants. Cardiovasc Diagn Ther. 2018;8:201–7. [PubMed: 30057869]
25. Boyden EA. Segmental anatomy of the lungs A Study of the Patterns of the Segmental Bronchi and Related Pulmonary Vessels. Pp. 42 McGraw-Hill Book Co. Inc.112s.BJS. 1955;43:108.
26. Brown RW, Cheng Y-CN, Haacke EM, Thompson MR, Venkatesan R. Magnetic resonance imaging : physical principles and sequence design; 2014.
27. Weaver KF, Morales VC, Dunn SL, Godde K, Weaver PF. An Introduction to Statistical Analysis in Research: With Applications in the Biological and Life Sciences: Wiley; 2017.
28. Akoglu H User's guide to correlation coefficients. Turkish Journal of Emergency Medicine. 2018;18:91–3. [PubMed: 30191186]
29. Marasini D, Quatto P, Ripamonti E. Assessing the inter-rater agreement for ordinal data through weighted indexes. Statistical methods in medical research. 2016;25:2611–33. [PubMed: 24740999]
30. Landis JR, Koch GG. The Measurement of Observer Agreement for Categorical Data. Biometrics. 1977;33:159–74. [PubMed: 843571]
31. Ohno Y, Nishio M, Koyama H, Yoshikawa T, Matsumoto S, Seki S, Sugimura K. Journal Club: Comparison of assessment of preoperative pulmonary vasculature in patients with non-small cell lung cancer by non-contrast- and 4D contrast-enhanced 3-T MR angiography and contrast-enhanced 64-MDCT. AJR Am J Roentgenol. 2014;202:493–506. [PubMed: 24555585]
32. Ohno Y, Yoshikawa T, Kishida Y, Seki S, Karabulut N. Unenhanced and Contrast-Enhanced MR Angiography and Perfusion Imaging for Suspected Pulmonary Thromboembolism. AJR Am J Roentgenol. 2017;208:517–30. [PubMed: 28075625]
33. Krishnam MS, Tomasian A, Deshpande V, Tran L, Laub G, Finn JP, Ruehm SG. Noncontrast 3D steady-state free-precession magnetic resonance angiography of the whole chest using nonselective radiofrequency excitation over a large field of view: comparison with single-phase 3D contrast-enhanced magnetic resonance angiography. Invest Radiol. 2008;43:411–20. [PubMed: 18496046]
34. Kanne JP, Lalani TA. Role of computed tomography and magnetic resonance imaging for deep venous thrombosis and pulmonary embolism. Circulation. 2004;109:I15–21. [PubMed: 15051664]
35. Fyrdahl A, Vargas Paris R, Nyren S, Holst K, Ugander M, Lindholm P, Sigfridsson A. Pulmonary artery imaging under free-breathing using golden-angle radial bSSFP MRI: a proof of concept. Magn Reson Med. 2018;80:1847–56. [PubMed: 29542200]
36. Tsao J, Kozerke S. MRI temporal acceleration techniques. J Magn Reson Imaging. 2012;36:543–60. [PubMed: 22903655]
37. Chamarthy MR, Kandathil A, Kalva SP. Pulmonary vascular pathophysiology. Cardiovasc Diagn Ther. 2018;8:208–13. [PubMed: 30057870]
38. Ehman RL, Felmlee JP. Adaptive technique for high-definition MR imaging of moving structures. Radiology. 1989;173:255–63. [PubMed: 2781017]
39. Bieri O, Scheffler K. Flow compensation in balanced SSFP sequences. Magn Reson Med. 2005;54:901–7. [PubMed: 16142709]
40. Heredia V, Altun E, Ramalho M, Campos R de, Azevedo R, Pamuklar E, Semelka RC. MRI of pregnant patients for suspected pulmonary embolism: steady-state free precession vs postgadolinium 3D-GRE. Acta Med Port. 2012;25:359–67. [PubMed: 23534587]
41. Choi K-J, Cha S-I, Shin K-M, Lim J-K, Yoo S-S, Lee J, et al. Factors determining clot resolution in patients with acute pulmonary embolism. Blood Coagul Fibrinolysis. 2016;27:294–300. [PubMed: 26484647]

42. Hosch W, Schlieter M, Ley S, Heye T, Kauczor H-U, Libicher M. Detection of acute pulmonary embolism: feasibility of diagnostic accuracy of MRI using a stepwise protocol. Emerg Radiol. 2014;21:151–8. [PubMed: 24282047]

43. Kalb B, Sharma P, Tigges S, Ray GL, Kitajima HD, Costello JR, et al. MR imaging of pulmonary embolism: diagnostic accuracy of contrast-enhanced 3D MR pulmonary angiography, contrast-enhanced low-flip angle 3D GRE, and nonenhanced free-induction FISP sequences. Radiology. 2012;263:271–8. [PubMed: 22438448]

44. Kaya F, Ufuk F, Karabulut N. Diagnostic performance of contrast-enhanced and unenhanced combined pulmonary artery MRI and magnetic resonance venography techniques in the diagnosis of venous thromboembolism. Br J Radiol. 2019;92:20180695. [PubMed: 30629460]

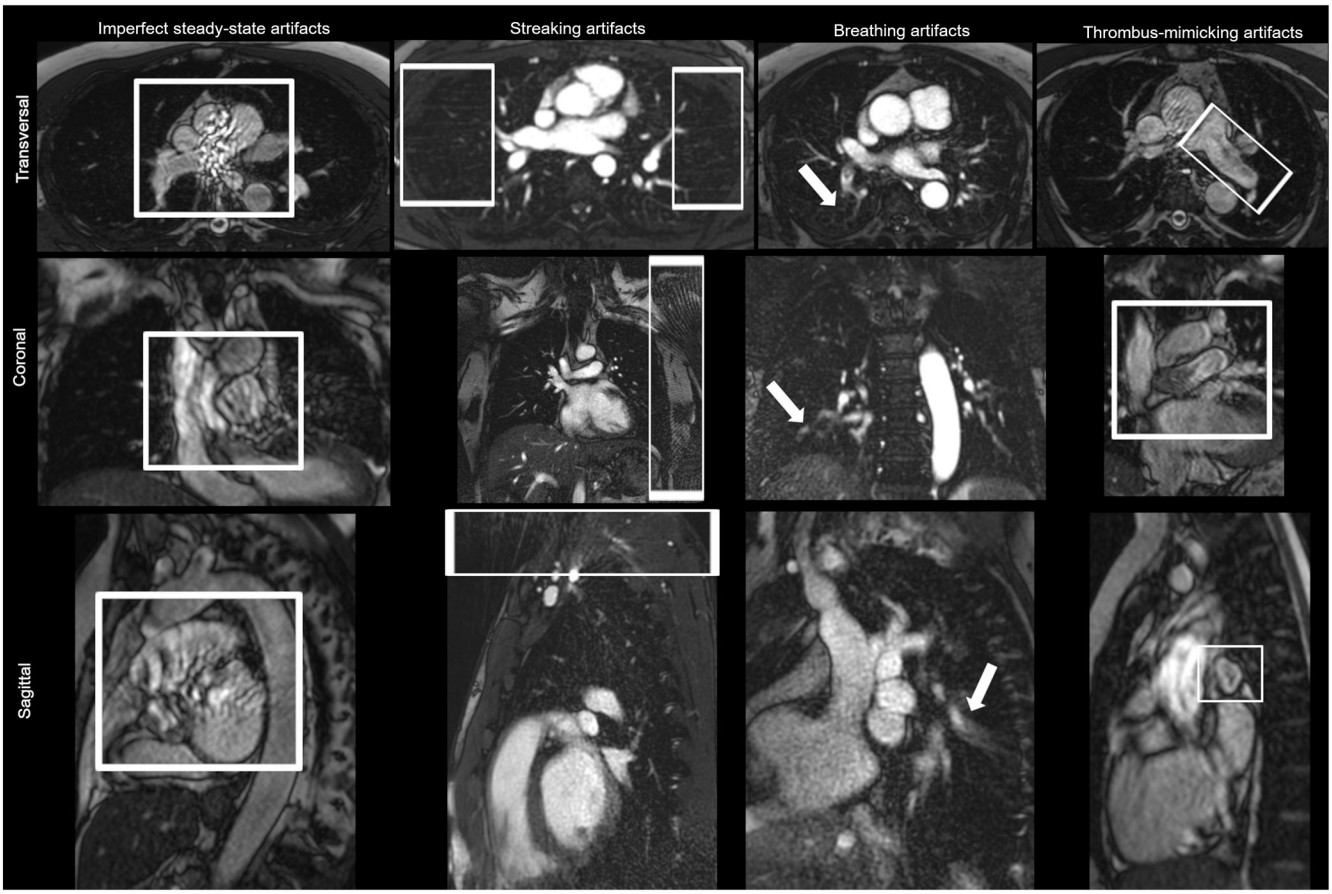

Figure 1: Exemplary views for evaluation of specific and general image artifacts.

The strongest degree of each artifact in different slice orientation is presented in this figure. The images presented for each artifact belong to a different healthy volunteer. For better visibility of the artifacts, the images were zoomed in or out in different ways.

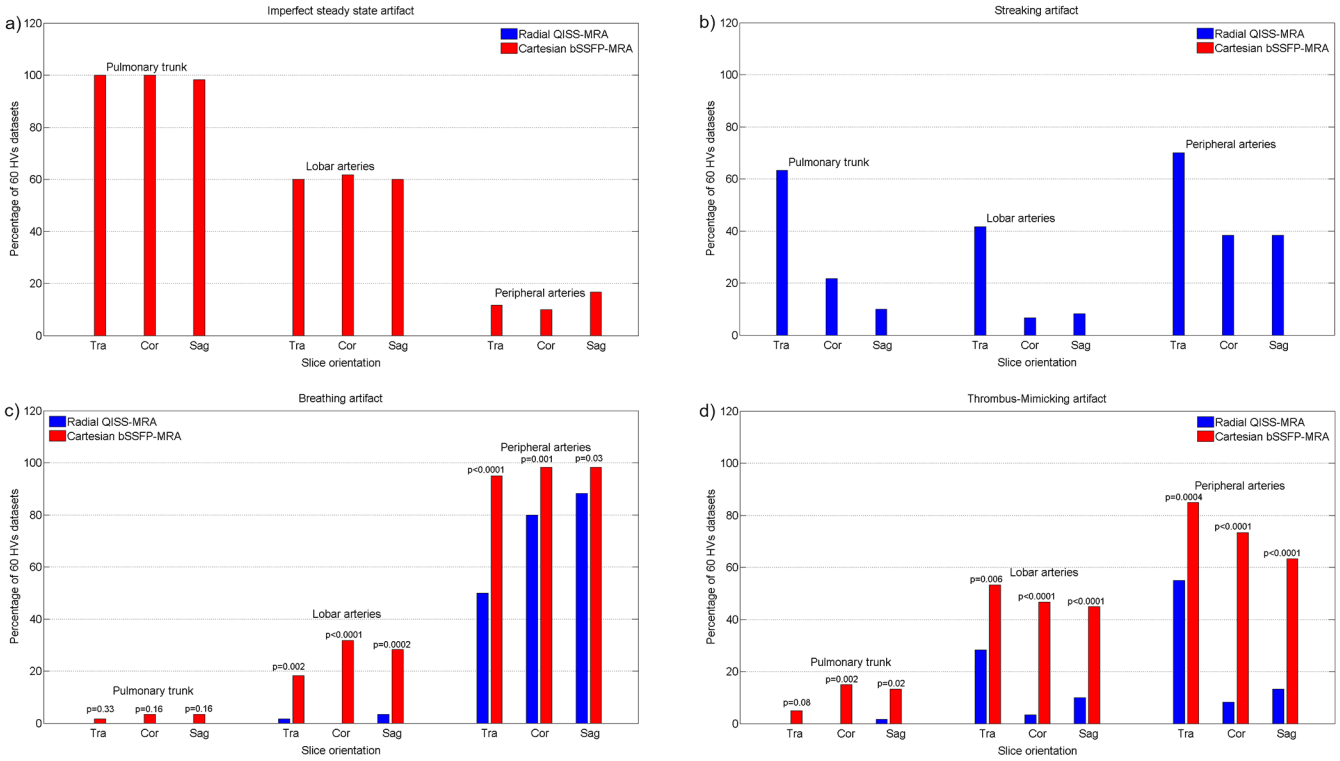

Figure 2: Evaluating the specific and general image artifacts in healthy volunteers (HV).

The percentage of occurrence of each imaging artifact is demonstrated as a function of slice orientation in three different pulmonary regions. The diagram is based on the results of the two readers together. The 60 datasets comprised 30 independently evaluated datasets of each radiologist.

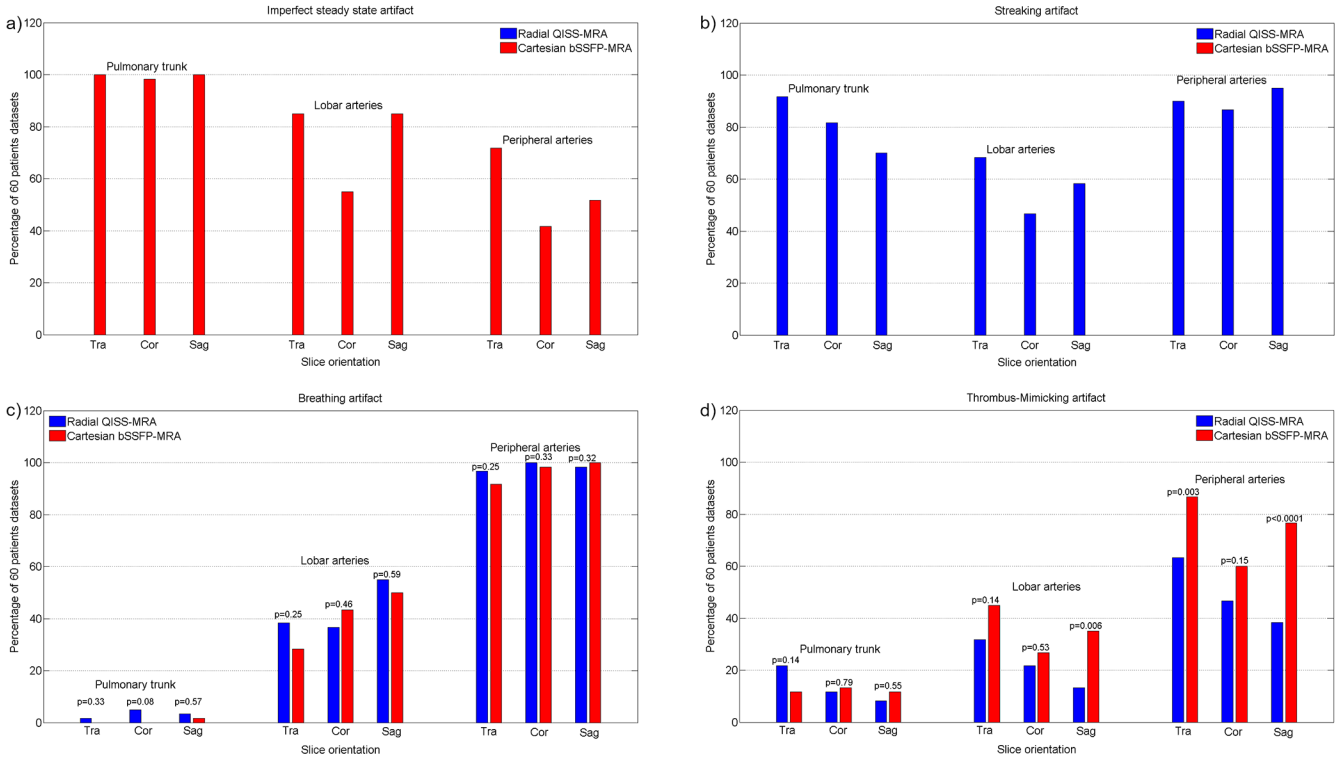

Figure 3: Evaluating the specific and general image artifacts in patients.

The percentage of occurrence of each imaging artifact is demonstrated as a function of slice orientation in three different pulmonary regions. The diagram is based on the results of the two readers together. The 60 datasets comprised 30 independently evaluated datasets of each radiologist.

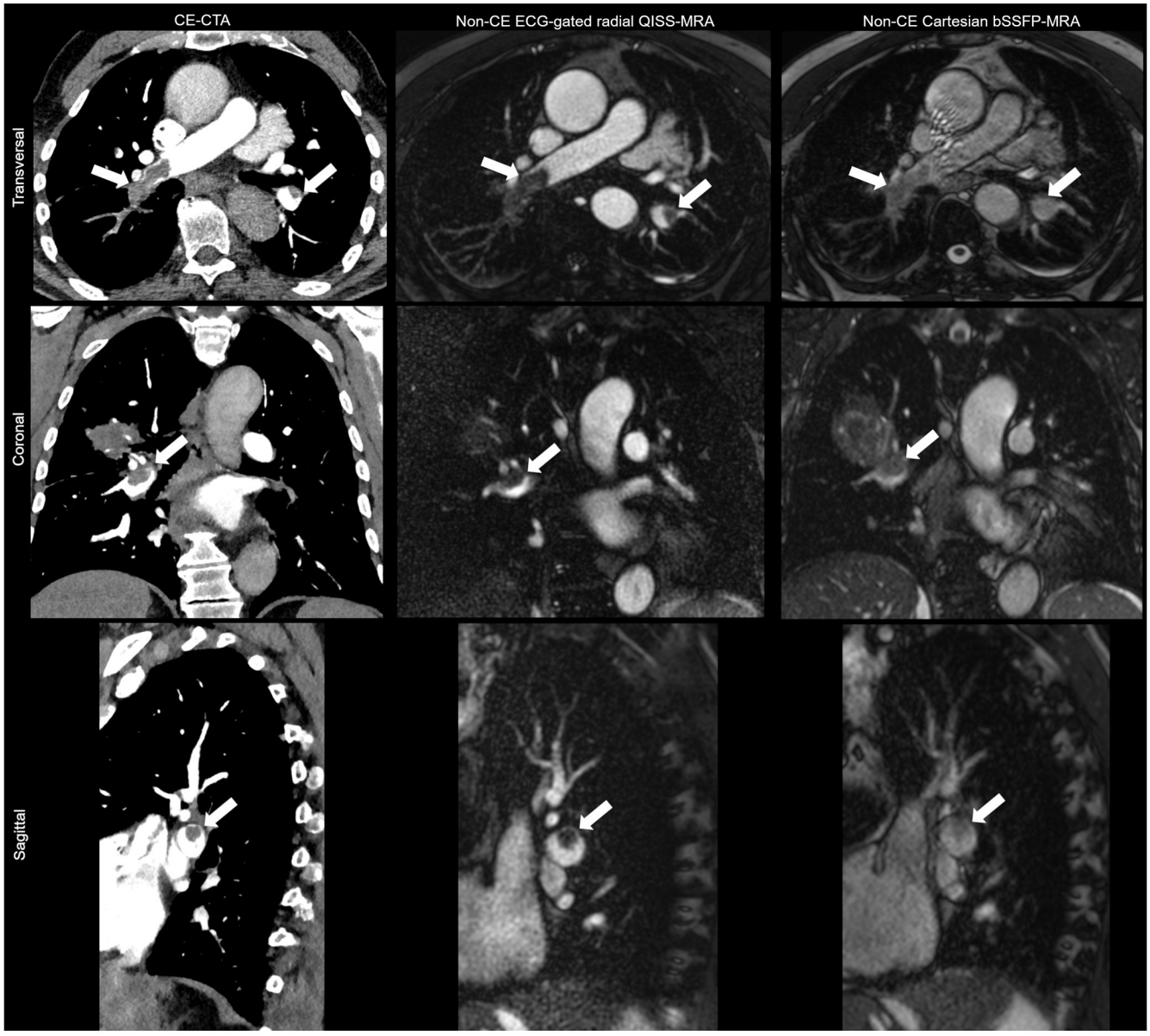

Figure 4: Exemplary views for the evaluation of arterial visualization and pulmonary artery embolism in patients with radial QISS, Cartesian bSSFP and CE-CTA.

The white arrows indicate the detected APE.

Table 1:

Demographic and clinical characteristic data of the study population.

All non-normally distributed continuous variables are given as median, first, and third quartile values. BMI: body mass index; n: number. The p-values refer to Wilcoxon signed-rank test.

	Patients (n = 30)	Healthy volunteers (n = 30)	p - value
Demographic data			
Female gender, n (%)	13 (43.3)	15 (50.0)	0.45
Age (years)	66.7 [62.3, 77.1]	42.4 [29.5, 53.5]	<0.0001
Weight (kg)	87.5 [72.8, 97.8]	80.0 [72.0, 90.8]	0.27
BMI (kg/m^2)	27.3 [24.8, 31.9]	26.1 [24.0, 28.4]	0.27
Referring site			
Outpatient	15 (50.0%)		
Inpatient	4 (13.3%)		
Emergency department	11 (36.7%)		
Indication for primary CE-CTA			
Tumor staging	15 (50.0%)		
Suspected acute pulmonary embolism	13 (43.3%)		
Exclusion of aortic dissection	1 (3.3%)		
Visualization of aortic aneurysm	1 (3.3%)		

Table 2:

Technical and clinical evaluation of radial QISS-MRA versus Cartesian bSSFP-MRA in healthy volunteers.

All non-normally distributed values are given as median, first, and third quartile values. Interquartile range is abbreviated to IQR. The evaluation of pulmonary arterial branches was based on the scoring systems introduced in the section “image analysis”. The p-values were determined using Wilcoxon signed-rank test. The significant p-values are marked in bold.

Variable	Radial QISS-MRA	Cartesian bSSFP-MRA	p-value
	Median (IQR)		
Signal-to-noise ratio (SNR)	227.5 (169.7, 286.3)	192.0 (160.1, 228.8)	0.09
Contrast-to-noise ratio (CNR)	216.6 (159.9, 273.6)	182.3 (152.1, 219.4)	0.09
Pulmonary arterial branches			
Truncus pulmonalis	4 (4, 4)	2 (2, 3)	**<0.0001**
Arteria pulmonalis dextra	4 (4, 4)	3 (3, 3)	**<0.0001**
Arteria pulmonalis sinistra	4 (4, 4)	3 (2, 3)	**<0.0001**
Right upper lobe	4 (3, 4)	3 (3, 3)	**<0.0001**
Left upper lobe	4 (3, 4)	3 (2, 3)	**<0.0001**
Right middle lobe	3 (3, 4)	3 (2, 3)	**<0.0001**
Right lower lobe	4 (4, 4)	3 (3, 3)	**<0.0001**
Left lower lobe	4 (3, 4)	3 (3, 3)	**<0.0001**
Right upper lobe apical	3 (3, 4)	3 (3, 3)	**<0.0001**
Right upper lobe posterior	3 (3, 4)	3 (3, 3)	**<0.0001**
Right upper lobe anterior	3 (3, 4)	3 (2, 3)	**<0.0001**
Left upper apicoposterior	4 (3, 4)	3 (2, 3)	**<0.0001**
Left upper lobe anterior	3 (3, 4)	3 (2, 3)	**<0.0001**
Left upper lobe lingular	3 (3, 4)	3 (2, 3)	**<0.0001**
Right middle lobe lateral	3 (3, 4)	3 (2, 3)	**<0.0001**
Right middle lobe medial	3 (3, 4)	3 (2, 3)	**<0.0001**
Right lower lobe superior	4 (3, 4)	3 (2, 3)	**<0.0001**
Right lower lobe medial	3 (3, 4)	3 (3, 3)	**0.0007**
Right lower lobe anterior	3 (3, 3)	3 (3, 3)	0.05
Right lower lobe lateral	3 (3, 3)	3 (3, 3)	**0.02**

Variable	Radial QISS-MRA	Cartesian bSSFP-MRA	p-value
	Median (IQR)		
Right lower lobe posterior	3 (3, 3)	3 (3, 3)	0.26
Left lower lobe superior	3 (3, 4)	3 (2, 3)	**<0.0001**
Left lower lobe anteromedial	3 (3, 3)	3 (2, 3)	**0.0002**
Left lower lobe lateral	3 (3, 4)	3 (3, 3)	**0.0009**
Left lower lobe posterior	3 (3, 4)	3 (3, 3)	**0.0005**

Table 3:

Technical and clinical evaluation of radial QISS-MRA versus Cartesian bSSFP-MRA in patients with acute pulmonary embolism.

All non-normally distributed values are given as median, first, and third quartile values. Interquartile range is abbreviated to IQR. The evaluation of pulmonary arterial branches was based on the scoring systems introduced in the section “image analysis”. The p-values were determined using Wilcoxon signed-rank test. The significant p-values are marked in bold.

Variable	Radial QISS	Cartesian bSSFP	p-value
	Median (IQR)		
Signal-to-noise ratio (SNR)	274.2 (220.8, 335.8)	205.7 (176.6, 253.4)	**0.03**
Contrast-to-noise ratio (CNR)	259.3 (213.8, 322.1)	195.1 (162.8, 240.8)	**0.02**
Pulmonary arterial branches			
Truncus pulmonalis	4 (4, 4)	3 (2, 3)	**<0.0001**
Arteria pulmonalis dextra	4 (3, 4)	3 (3, 3)	**<0.0001**
Arteria pulmonalis sinistra	4 (4, 4)	3 (3, 3)	**<0.0001**
Right upper lobe	4 (3, 4)	3 (2, 3)	**<0.0001**
Left upper lobe	4 (3, 4)	3 (2, 3)	**<0.0001**
Right middle lobe	3 (3, 3)	2 (2, 3)	**<0.0001**
Right lower lobe	3 (3, 4)	3 (2, 3)	**<0.0001**
Left lower lobe	4 (3, 4)	3 (3, 3)	**<0.0001**
Right upper lobe apical	3 (3, 4)	2 (2, 3)	**<0.0001**
Right upper lobe posterior	3 (2, 3)	2 (2, 3)	**<0.0001**
Right upper lobe anterior	3 (3, 4)	2 (2, 3)	**<0.0001**
Left upper lobe apicoposterior	3 (3, 3)	2 (2, 3)	**<0.0001**
Left upper lobe anterior	3 (3, 3)	2 (2, 3)	**<0.0001**
Left upper lobe lingular	3 (3, 3)	2 (2, 2)	**<0.0001**
Right middle lobe lateral	2 (2, 3)	2 (2, 3)	**0.04**
Right middle lobe medial	3 (2, 3)	2 (2, 3)	**<0.0001**
Right lower lobe superior	3 (2, 3)	2 (2, 3)	**<0.0001**
Right lower lobe medial	3 (2, 3)	2 (2, 3)	**<0.0001**
Right lower lobe anterior	3 (2, 3)	2 (2, 3)	**0.009**
Right lower lobe lateral	3 (2, 3)	2 (2, 3)	**0.0005**

Variable	Radial QISS	Cartesian bSSFP	p-value
	Median (IQR)		
Right lower lobe posterior	3 (2, 3)	2 (2, 3)	**0.006**
Left lower lobe superior	3 (3, 3)	2 (2, 3)	**<0.0001**
Left lower lobe anteromedial	3 (2, 3)	2 (2, 3)	**0.0005**
Left lower lobe lateral	3 (3, 3)	2 (2, 3)	**0.0003**
Left lower lobe posterior	3 (3, 3)	2 (2, 3)	**0.0005**

Table 4:

Correlation between MRA methods and CE-CTA concerning the accurate determination of APE grading (Grades 0, 1, and 2).

The r-value indicates the Spearman's correlation coefficient, and p-values show whether the correlation coefficient is significantly different from 0.

	Radial QISS-MRA vs. CE-CTA	Cartesian bSSFP-MRA vs. CE-CTA	Radial QISS vs. Cartesian bSSFP-MRA
Pulmonary arterial regions	**r-value p-value**		
Central arteries	0.88 <0.0001	0.74 <0.0001	0.79 <0.0001
Lobar arteries	0.88 <0.0001	0.70 <0.0001	0.76 <0.0001
Peripheral arteries	0.82 <0.0001	0.67 <0.0001	0.69 <0.0001

Table 5:

Diagnostic performance of MRA methods versus CE-CTA of the two readers.

Data are percentages; 95% confidence intervals are provided in parentheses.

Variable (%)	Sensitivity	Specificity	Positive predictive value	Negative predictive value	Accuracy
MRA methods					
Radial QISS-MRA					
Central arteries	89.7 (72.7 – 97.8)	98.1 (94.4 – 99.6)	89.7 (73.7 – 96.4)	98.1 (94.5 – 99.3)	96.7 (93.0 – 98.8)
Lobar arteries	94.6 (89.1 – 97.8)	93.0 (88.1 – 96.3)	91.0 (85.5 – 94.6)	95.8 (91.7 – 97.9)	93.7 (90.3 – 96.1)
Peripheral arteries	84.9 (81.5 – 88.0)	92.2 (89.7 – 94.3)	90.6 (87.8 – 92.8)	87.4 (84.9 – 89.6)	88.8 (86.8 – 90.6)
All pulmonary arterial branches	**86.0 (83.0 – 88.6)**	**93.4 (91.5 – 94.9)**	**89.9 (87.5 – 92.0)**	**90.6 (88.8 – 92.2)**	**90.4 (88.8 – 91.8)**
Cartesian bSSFP					
Central arteries	76.9 (56.4 – 91.0)	98.7 (95.4 – 99.8)	90.9 (71.3 – 97.6)	96.2 (92.6 – 98.1)	95.6 (91.4 – 98.1)
Lobar arteries	82.7 (75.0 – 88.8)	85.0 (78.8 – 89.9)	80.2 (73.7 – 85.3)	87.0 (82.0 – 90.8)	84.0 (79.4 – 88.0)
Peripheral arteries	75.6 (71.3 – 79.5)	83.8 (80.5 – 86.7)	78.4 (74.9 – 81.5)	81.5 (78.9 – 83.9)	80.2 (77.6 – 82.6)
All pulmonary arterial branches	**80.6 (77.5 – 83.5)**	**86.6 (84.2 – 88.7)**	**82.5 (79.9 – 84.8)**	**85.1 (83.0 – 86.9)**	**84.0 (82.1 – 85.7)**

Table 6:

Interobserver and intraobserver agreement for the clinical evaluation of radial QISS-MRA and Cartesian bSSFP.

Data are given as agreement, and 95% confidence interval values are in parentheses.

Variable	Patients	
	Radial QISS-MRA	Cartesian bSSFP
Interobserver agreement		
Visualization of anatomical segmentations		
Central region	0.88 (0.84 – 0.92)	0.88 (0.85 – 0.92)
Lobar region	0.71 (0.63 – 0.80)	0.79 (0.75 – 0.84)
Peripheral region	0.83 (0.80 – 0.87)	0.80 (0.77 – 0.82)
Diagnostic of acute pulmonary embolism		
Central region	0.97 (0.93 – 0.99)	0.97 (0.93 – 0.99)
Lobar region	0.95 (0.92 – 0.98)	0.90 (0.86 – 0.94)
Peripheral region	0.89 (087 – 0.92)	0.81 (0.78 – 0.85)
Intraobserver agreement		
Visualization of anatomical segmentations		
Central region		
Reader 1	0.98 (0.96 – 1.00)	0.94 (0.92 – 0.97)
Reader 2	0.97 (0.95 – 0.99)	0.98 (0.96 – 1.00)
Lobar region		
Reader 1	0.82 (0.78 – 0.86)	0.89 (0.86 – 0.92)
Reader 2	0.91 (0.88 – 0.93)	0.89 (0.86 – 0.92)
Peripheral region		
Reader 1	0.87 (0.85 – 0.89)	0.86 (0.85 – 0.88)
Reader 2	0.86 (0.83 – 0.89)	0.92 (0.91 – 0.94)
Diagnostic of acute pulmonary embolism		
Central region		
Reader 1	0.98 (0.96 – 1.00)	0.99 (0.98 – 1.00)
Reader 2	0.98 (0.96 – 1.00)	0.99 (0.98 – 1.00)

Variable	Patients	
	Radial QISS-MRA	Cartesian bSSFP
Lobar region		
Reader 1	0.96 (0.93 – 0.99)	0.91 (0.87 – 0.95)
Reader 2	0.98 (0.96 – 1.00)	0.92 (0.89 – 0.96)
Peripheral region		
Reader 1	0.93 (0.91 – 0.95)	0.92 (0.91 – 0.94)
Reader 2	0.97 (0.95 – 0.99)	0.86 (0.83 – 0.90)